



Article

An Improved Retrieval Method for *Porphyra* Cultivation Area Based on Suspended Sediment Concentration

Yinhe Cheng ^{1,*}, **Yue Sun** ¹, **Lin Peng** ¹, **Yijun He** ² and **Mengling Zha** ¹¹ School of Marine Technology and Geomatics, Jiangsu Ocean University, Lianyungang 222005, China² School of Marine Sciences, Nanjing University of Information Science and Technology, Nanjing 210044, China

* Correspondence: chengyh@jou.edu.cn

Abstract: The rapid expansion of *Porphyra* farming in China lends considerable urgency to developing a satellite remote sensing retrieval method to monitor its cultivation, in order to promote sustainable economic development and protective utilization of ecosystem-oriented marine natural resources. For medium-resolution satellite imagery such as HY-1C images, pixel-by-pixel techniques are appropriate; however, many factors affect the retrieval accuracy of the *Porphyra* cultivation area. In coastal regions, *Porphyra* and suspended sediment radiate a similar spectrum, which inevitably causes errors in the identification of the *Porphyra*. To improve the overall retrieval accuracy of *Porphyra* cultivation area from medium-resolution HY-1C images, we considered suspended sediment concentration (SSC) as an independent variable and constructed a new model in conjunction with high-resolution Sentinel-2 satellite images using a linear regression method in Haizhou Bay, China. A comparative analysis was performed with a traditional random forest classification algorithm and pixel-based dichotomy model in different SSC seawater. The results showed that the new model expressed the best ability to supervise *Porphyra* cultivation area, and its overall relative error and root mean square deviation, whether in area or in validation sample points, were the lowest among the models. The experiment was performed by removing the SSC variable while using the same processes as in the new model, and the results indicate that the SSC played an important role in new model, which is suitable to be applied to coastal seawater containing more suspended sediment, as in the HY-1C coastal zone image. The application of the new model on temporal change in the retrieved results was indirectly verified as effective. This study provides an effective method to exactly extract *Porphyra* cultivation area in the coastal sea using medium-resolution HY-1C satellite imagery.



Citation: Cheng, Y.; Sun, Y.; Peng, L.; He, Y.; Zha, M. An Improved Retrieval Method for *Porphyra* Cultivation Area Based on Suspended Sediment Concentration. *Remote Sens.* **2022**, *14*, 4338. <https://doi.org/10.3390/rs14174338>

Academic Editors: Assefa M. Melesse and Giovanni Battista Chirico

Received: 23 June 2022

Accepted: 25 August 2022

Published: 1 September 2022

Publisher's Note: MDPI stays neutral with regard to jurisdictional claims in published maps and institutional affiliations.



Copyright: © 2022 by the authors. Licensee MDPI, Basel, Switzerland. This article is an open access article distributed under the terms and conditions of the Creative Commons Attribution (CC BY) license (<https://creativecommons.org/licenses/by/4.0/>).

1. Introduction

Aquaculture, the commercial raising of aquatic organisms, is an important part of the world's food production structure. *Porphyra* is one of the most ubiquitous of the aquacultures for human consumption in East Asia. According to the Food and Agriculture Organization, it is among the most nutritious seaweeds, with a protein content of 30–50 percent, and about 75 percent of that is digestible [1]. Therefore, China's aquaculture industry has maintained steady growth and become an important economic and food source for its coastal cities in recent years [2]. *Porphyra* is one of the largest mariculture industry in China. Based on the data from China Fishery Statistical Yearbook during the period of 2013–2020, the annual production of *Porphyra* has continuously increased every year and in 2020, China produced 222,000 tons of *Porphyra*, which is an increase of 4.57% over 2019 [3].

Because of its economic importance and health benefits, *Porphyra* in Lianyungang is becoming an important pillar of the marine economy in Jiangsu Province [4]. *Porphyra* farming in Lianyungang coastal region is expanding and extending into the deep sea [5,6].

The rapid expansion of the *Porphyra* cultivation brings a series of environmental and ecological problems in the local sea region, such as eutrophication of water bodies and destruction of pristine water ecology [7–10]. It was reported that the gradual expansion of *Porphyra* cultivation area in Jiangsu coast might lead to green tide occurrence in the Yellow Sea [11,12]. In short, marine environmental monitoring requirements, spatial planning enforcement and ecosystem-oriented natural resources management lend considerable urgency to the development of operation solutions that can extract tangible information from remote-sensing images to promote sustainable economic development and protective utilization of marine resources in China.

Remote-sensing technology has become important and indispensable, and many retrieval methods have been researched and applied to detect aquaculture areas. Three main types of image classification techniques have been developed in the remote-sensing field, namely unsupervised image classification, supervised image classification, and object-based image analysis. Unsupervised and supervised image classification are usually available in the category of per-pixel classification for low spatial resolution images, and the supervised classification methods have been validated in the extraction of *Porphyra* cultivation area or aquaculture area from remote sensing images [13–15]. For example, Zhou et al. analyzed the aquaculture information of the estuary of Jialongjiang River using two classification approaches from ASTER images [16].

Another image classification is object-based image analysis (OBIA), which is more popular in present times and is summarized in the literature [17]. OBIA segments an image by grouping pixels and builds on edge-detection, feature extraction, and classification concepts for the high spatial resolution image. Thus, it is often applied for the identification of aquaculture cultivation area [18–25]. In this method, human–computer interaction and visual interpretation is usually adopted to obtain useful information from remote-sensing data based on the field survey and personal expertise or knowledge for the aquaculture cultivation area [18–20]. However, the scale of the object segment is subjectively affected by the individual researcher, which has a certain influence on the accuracy. Thus, associated rules to find the relationships, such as correlations and co-occurrences between data items, are documented to reduce the effect of the subjective factor on remote-sensing identification and improve the retrieval accuracy of *Porphyra* cultivation areas [26,27].

Pixel-based detection or object-based image analysis is usually regionalization approach using different algorithms or data processes to monitor the *Porphyra* cultivation areas. Guo et al. demonstrated that the overall accuracy of *Porphyra* cultivation area retrieval was improved using the normalized difference vegetation index (NDVI) compared with the difference vegetation index (DVI) [28]. Wei et al. analyzed the distribution of *Porphyra* cultivation areas in Haizhou Bay during the period 2000–2015 based on NDVI [22] and Lu et al. investigated the expansion of *Porphyra* cultivation areas in Haizhou Bay using NDVI and mean spectral feature [6,21]. Similarly, DVI was used by Xing et al. to extract *Porphyra* cultivation areas in this sea region from high-resolution images [29]. It has been frequently claimed that spatial resolution is crucial to these methods [17] and these reports focused on high spatial resolution images from Gaofen-1, Sentinel-1, Landsat and SPOT satellites and so on.

HY-1C, China's independent research ocean satellite, was officially put into service on 28 June 2019. Its Coastal Zone Imager (CZI) is mainly designed to supervise vegetation and the coastal zone in real-time, and has 50 m resolution from space [30]. Since a single farming region consisting of several rows of racks in Haizhou Bay is close to a square in shape with each side having a length of 80–120 m [24], the pixel of the HY-1C image and the object size are of the same order, which yields many mixed pixels. To deal with fuzzy objects or fields in space, special techniques are applied such as hybrid image element decomposition [31–33] and regional regression models [13,34] to estimate relevant vegetation parameters. These algorithms are rarely used to investigate the *Porphyra* cultivation areas. Additionally, significant suspended sediment exists in the coastal seawater of Haizhou Bay and is sensitive to the red and near-infrared bands [35,36]; *Porphyra* has the same spectral features

through DVI, which brings some difficulties to the remote-sensing retrieval of *Porphyra* cultivation areas.

Although Wang et al. combined NDVI with a dynamic threshold to monitor the *Porphyra* cultivation areas in Haizhou Bay from HY-1C CZI [25], the retrieval accuracy was not estimated and the problem caused by mixed pixel is not considered. Consequently, in order to fully use HY-1C CZI to derive exact *Porphyra* cultivation area, taking the near-shore *Porphyra* farming area in Haizhou Bay as an example, we propose a new empirical inversion algorithm for *Porphyra* cultivation area through fractional vegetation cover (FVC) obtained from Sentinel-2 images, and introduce three other pre-pixel compared methods in Section 2. The remainder of this paper is arranged as follows. Section 3 gives the results of comparative analysis and discusses suspended sediment effects on the new model. The conclusions are summarized in Section 4.

2. Data and Methods

2.1. Study Area

In this paper, remote-sensing inversion experiments were carried out on the *Porphyra* cultivation in the coastal waters of Haizhou Bay, near Lianyungang, China. The geographical location of the study region is shown in Figure 1.

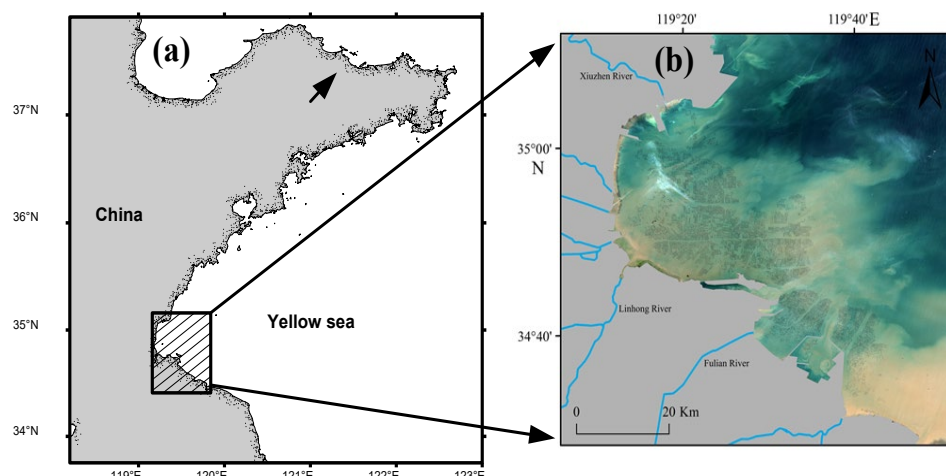


Figure 1. (a) Location of study region with hatching added. The true color image (b) in the sea is a composite of Sentinel-2 spectral Band 2, Band 3, and Band 4 on 12 January 2020, and the gray segments show the patches of lands.

Haizhou Bay is a semi-enclosed bay in the Yellow Sea (Figure 1a) where there are several rivers entering the sea, such as the Fulian River and Linlong River in Figure 1b. Thus, significant suspended sediment is brought into the bay by the rivers. The uneven distribution far away from the coast as shown in Figure 1b is bound to affect remote-sensing monitoring of *Porphyra*. This is why we introduce the SSC to model building to try to decrease the error of the retrieval algorithm.

Additionally, the growth of *Porphyra* is affected by seawater temperature, and its relative growth rate is higher when the seawater temperature is lower than 6 °C [15]. Therefore, the culture time of *Porphyra* in Haizhou Bay is mainly concentrated from November to March, which is its growing season. In the early months, seedlings are cultured using the fixed pole method in Haizhou Bay. The racks consist of two rows, each with nine or more long bamboo poles that are driven into the sea bed, and the poles are placed so that a stretched net fits precisely between them. Usually, eight or more such rows are placed next to each other so that most of the poles serve two nets. Thus, this forms a nearly square area of *Porphyra* cultivation, with each side about 80–120 m. The plants are tied on the nets and grow rapidly, requiring about 45 days from seeding until the first harvest. The

remaining thalli are allowed to grow for a second harvest after another 15–20 days, and several harvests are made from the same nets in one growing season [37].

2.2. Remote-Sensing Data

Two kinds of satellite data were employed to build the empirical regression model of the *Porphyra* cultivation to improve the accuracy of remote-sensing retrieval from HY-1 images. Table 1 lists the main technical parameters of the two satellite sensors.

Table 1. Specification of the two satellite sensors.

Sensor	Bands	Wavelength Range (μm)	Spatial Resolution (m)	Swath Width (km)	Revisit Period (days)
HY-1C	1–Blue	0.420–0.500	50	950	3
	2–Green	0.520–0.600			
	3–Red	0.610–0.690			
	4–NIR *	0.760–0.890			
Sentinel-2	2–Blue	0.459–0.525	10	290	5
	3–Green	0.541–0.577			
	4–Red	0.649–0.684			
	8–NIR *	0.780–0.886			

* NIR is short for near infrared band.

Table 1 shows that each satellite carries a single multi-spectral instrument (MSI) deploying 4 spectral channels in the visible/near infrared bands and that they have different spatial resolution: 50 m for HY-1C and 10 m for Sentinel-2. Thus, the pixel resolution in the case of Sentinel-2 is one that 25th of the HY-1C and the high-resolution data from Sentinel-2 can help us to improve remote-sensing retrieval accuracy from HY-1C image data through the FVC parameter. According to *Porphyra* growth stages, six images of Haizhou Bay were employed; Table 2 lists the detailed introduction.

Table 2. Images from the two satellites used in this study.

NO. of Images	Date of HY-1C CZI	Date of Sentinel-2 Images	Data Usage
1	31 January 2020	12 January 2020	Building models and validating and assessing the models
2	9 February 2020	16 February 2020	Time series application for the new model and assessing model indirectly
3	19 March 2020	16 February 2020	

HY-1C images were download from the National Satellite Ocean Application Center of China website (<https://osdds.nsoas.org.cn> (accessed on 1 May 2020)) and the product type was the L1B level. The Sentinel 2 data were derived from the United States Geological Survey website (USGS) (<https://earthexplorer.usgs.gov> (accessed on 1 May 2020)). The two images were matched according to the observed date. Additionally, those images are cloud-free in Haizhou Bay during the observation periods, which removes significant noise caused by clouds and their shadows for image analysis and applications.

2.3. Methods

A new empirical model was developed using matched satellite imagery of HY-1C and Sentinel-2, in consideration of suspended sediment as a key factor with the least-squares method. Another method without SSC was the comparative model. Since the spectral features of *Porphyra* as an aquatic plant have some similarities with terrestrial vegetation, the traditional random forest classification algorithm was used for comparative analysis in this study. Besides this method, another comparative approach was a pixel-based dichotomy model, which is widely used in remotely sensed land cover classification. In this method, the concept of fractional vegetation cover (FVC) is introduced and defined

as the percentage of the total study area that is vegetated [38], in order to reduce errors in remote-sensing monitoring caused by mixed pixels. Therefore, this pixel-based dichotomy model was employed as a comparative method. Figure 2 shows the flow chart of the research in this study.

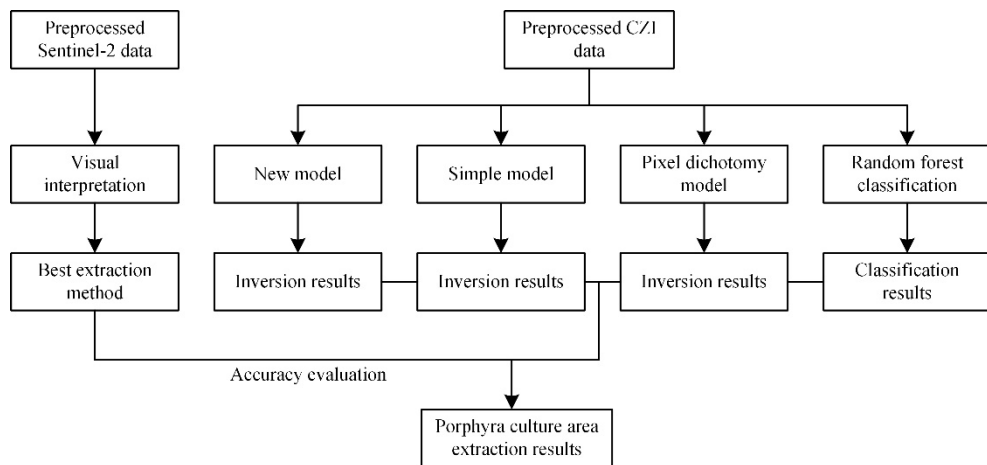


Figure 2. The research flow chart.

2.3.1. Data Preprocessing

Data pre-processing includes geometric and radiometric calibration. Sentinel-2 data pre-processing was mainly done using Sen2cor software. For the HY-1C images, the L1B data of HY-1C are stored in the HDF5 format, and we obtained the parameter information by searching the attribute table. The geometry correction was done by inputting the geometry file of the HY-1C data to generate a geographic location lookup table file. Then, spectral irradiance of the L1B data was converted into apparent reflectance through the radiometric calibration process [39],

$$\rho = \frac{\pi \cdot L_\lambda \cdot D^2}{ESUN_\lambda \cdot \cos \theta} \quad (1)$$

where ρ is the apparent reflectance (dimensionless), L_λ is the spectral radiance in $W/(m^2 \cdot \mu m \cdot Sr)$, D is the solar-terrestrial distance in astronomical units, $ESUN_\lambda$ is the solar mean spectral irradiance in $W/(m^2 \cdot \mu m)$, and θ is the solar zenith angle.

2.3.2. Vegetation Index Calculation

The main indices involved in the models were all normalized, including the vegetation index, normalized water index, and suspended sediment concentration index, since *Porphyra* is a plant and has a similar spectral feature with terrestrial vegetation. It is more sensitive to the near-infrared (NIR) band, and NDVI is usually used in vegetation remote sensing [40]. Considering the spectral features of the seawater body, the normalized difference water index (NDWI) was used [41] and the SSC was derived from the literature [42]. Three indices were calculated as follows,

$$NDVI = \frac{R_{NIR} - R_{RED}}{R_{NIR} + R_{RED}} \quad (2)$$

$$NDWI = \frac{R_{GREEN} - R_{NIR}}{R_{GREEN} + R_{NIR}} \quad (3)$$

$$SSC = 64.54 - 7033.83 \times R_{RED} + 96027 \times R_{NIR} \quad (4)$$

where R_{NIR} , R_{RED} , and R_{GREEN} represent the near-infrared band, the red band, and the green band, respectively. SSC is the suspended sediment concentration ($mg \cdot L^{-1}$) and its

formula (4) was obtained from HY-1C data and observed data, which has good applicability in the Yangtze estuary seawaters [42].

NDVI, NDWI, and SSC have different scale units and differences in magnitude. In order to further apply these parameters and obtain reliable results, a z-score standardization method was employed to process the data; the conversion function is as follows [8],

$$x^* = \frac{x - \bar{x}}{\sigma} \quad (5)$$

where \bar{x} is the mean of the original data and σ is the standard deviation of the original data.

2.3.3. Random Forest Classification Model

The random forest classification model is a specific supervised model that depends on decision trees, ensemble models, and bootstrapping three processes. Decision trees are used for both regression and classification problems. They visually flow like trees, and can be applied in the classification case for remote-sensing images [43]. Based on this algorithm, NDVI and NDWI were calculated from HY-1C image data to accomplish classification of *Porphyra* cultivation area.

2.3.4. Pixel-Based Dichotomy Model

The pixel-based dichotomy model is usually used for a single image element with bare soil and vegetation. Thus, the FVC can be derived from an image element based on a simple physical model to reduce the influence of mixed pixels on target extraction [14]. Since a single pixel composition in sea with seawater and *Porphyra* area is similar to land, this classification method was proposed and applied for the mixed pixels of cultivation area, based on different spectral features of the seawater and *Porphyra*. The FVC index was calculated using following formula from the literature [9],

$$FVCI = \frac{NDVI - NDVI_{seawater}}{NDVI_{Porphyra} - NDVI_{seawater}} \quad (6)$$

where $NDVI_{seawater}$ and $NDVI_{Porphyra}$ are the typical NDVI values of seawater and *Porphyra* cultivation area, which were derived from the average NDVIs of each 10,000 pixels of seawater and cultivation area samples in the same HY-1C image in Haizhou Bay.

2.3.5. New and Simple Model

Since remote-sensing retrieval methods are empirical or semi-empirical algorithms, a new model was built with the Sentinel-2 multispectral sample points to correct the retrieval from the HY-1C image. First, *Porphyra* cultivation area was retrieved from Sentinel-2 multispectral data by visual interpretation of the observed data in Haizhou Bay, because it has a high spatial resolution of 100 m^2 in area. The retrieved results from the Sentinel-2 image were recorded; *Porphyra* cultivation area as 1 and seawater as 0. Then, these data were used for the empirical model construction and validation. Secondly, this observed dataset was matched with HY-1C image data using a location mapping technology from geographic information systems (GIS). A pixel of the HY-1C image has a spatial resolution of 2500 m^2 in area and thus, it corresponds to 25 Sentinel-2 pixels. In this way, we obtained 260,000 sample points of HY-1C image by geographic coordinate matching. Because of the spatial resolution of different satellite imagery, the proportion of the *Porphyra* cultivation was derived from the Sentinel-2 observed data, which was the FVC applied to build models and improve retrieval accuracy.

Combining retrieved information from the HY-1C pixels with the corresponding FVC, relations were built with the least square method, and two linear regression statistical models were obtained; one, called “new model”, considered the effect of suspended sediment, and the other, called “simple model” lacked the SSC to serve as the contrast experiments. The simple model was based on NDVI and NDWI and the new model was

closely related to NDVI, NDWI, and SSC. We compared the two models to investigate the effect of suspended sediment on the retrieval accuracy of *Porphyra* cultivation area.

Finally, the matched points were randomly divided into two groups and 60% of the sample points were taken to build the models. The remainder was used to validate and assess the models. Then, based on the first group of 60% of the sample points, two multi-parameter linear regression models were obtained using the least-squares method. The FVC of the new model is the function of the selectable NDVI, NDWI, and SSC extracted from the HY-1C image, and the simple model is similar but with the SSC removed. These models are as follows:

$$\text{Simple model: } \text{FVC}_1 = 1.235 \times \text{NDVI} - 0.758 \times \text{NDWI} + 0.077 \quad (7)$$

$$\text{New model: } \text{FVC}_2 = 0.674 \times \text{NDVI} - 0.177 \times \text{NDWI} - 0.772 \times \text{SSC} + 0.7 \quad (8)$$

2.3.6. Accuracy Assessment Parameters

There were four methods to derive the area of *Porphyra* farming for the comparative analysis. The cultivation area of *Porphyra* in Haizhou Bay was calculated by Formula (10):

$$S = \sum_{i=1}^N \text{FVC}_i \times 50^2 \times 10^{-6} \quad (9)$$

where S is area in km^2 and FVC_i is the proportion of the i -th pixel in the HY-1C image. N is the total number of FVC pixels for the study region. It is worth noting that the results retrieved by the pixel-based dichotomy model contain abnormal values, so each abnormal FVC value from the HY-1C image is converted into two values, 0 if $\text{FVC} < 0$ and 1 if $\text{FVC} > 1$. Thus, FVC values from the HY-1C image were discrete numbers in [0, 1].

Two parameters were used to evaluate the models. One is relative error (RE) and the other is root mean square error (RMSE), which were used as evaluation metrics, with RE and RMSE calculated by Formula (10) [23] and Formula (11) [22], respectively:

$$\text{RE} = \frac{\left| \sum_{i=1}^N O_i - \sum_{i=1}^N M_i \right|}{\sum_{i=1}^N O_i} \times 100\% \quad (10)$$

$$\text{MSE} = \left(\sum_{i=1}^n (e_i)^2 / N \right)^{1/2} \quad (11)$$

where O_i is the observed value, namely, the total area of *Porphyra* cultivation or the total FVC of the corresponding 25 pixels of the Sentinel-2 image, and M_i is the model value obtained from the HY-1C CZI. e_i is the absolute difference between the observed and model values, and N is the number of validation sample points from the HY-1C image.

3. Comparative Analysis with Other Three Models

3.1. Accuracy Assessment of *Porphyra* Cultivation Area Retrieved from Sentinel-2 Image

Since the image from Sentinel-2 was used to build the new model and the comparative model, its retrieved accuracy of *Porphyra* cultivation area needed to be assessed. A total of 1000 pixel samples were randomly generated in the Sentinel-2 satellite image acquired on 12 January 2020 and divided into two categories by visual interpretation, which were *Porphyra* cultivation area and seawater. Then, each sample location of each group was checked and identified again as the true value using image processing techniques for the Sentinel-2 image. Thus, we carried out an accuracy assessment for two classifications using the user's and producer's accuracy, overall accuracy, and the Kappa coefficient of agreement. Table 3 summarizes the accuracy assessment.

Table 3. Accuracy assessment of the two classifications for Sentinel-2 image.

	Category	PCA	Actual Value * SW	Total	UA(%)
Visual interpretation resamples	PCA	336	20	356	94.3
	SW	18	626	644	97.2
	Total	354	646	1000	—
	PA/%	95.0	97.0	—	—
	OA/%	—	—	96.2	—
	Kappa	—	—	0.92	—

* PCA: *Porphyra* cultivation area; SW: sea water; UA: user's accuracy; PA: producer's accuracy; OA: overall accuracy.

From Table 3, the classification of the Sentinel-2 image by visual interpretation exhibits the highest classification accuracy, with an overall of 96.2% and a Kappa of 0.92, and the producer's accuracy of *Porphyra* cultivation area also reaches about 95.0%. The results indicate that for this high spatial resolution image, the retrieved *Porphyra* cultivation areas from the Sentinel-2 images were considered the true values. Then, we used the Sentinel-2 data with similar process to build and validate models.

3.2. Analysis of the Qualitative Impact

According to Formula (4), the distribution of SSC was retrieved from the HY-1C image on 31 January 2020 in Haizhou Bay, as shown in Figure 3. It shows a decreasing trend of suspended sediment content from coast to open sea, which is consistent with the basic characteristics of suspended sediment distribution in Haizhou Bay.

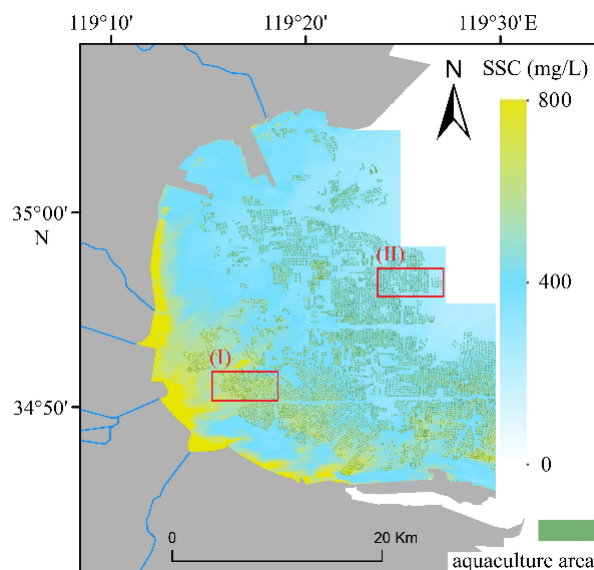


Figure 3. Distribution of SSC retrieved from HY-1C image on 31 January 2020 in Haizhou Bay. (I) high concentration region with SSC greater than 500 mg/L and (II) low concentration region with SSC less than 400 mg/L.

The retrieved FVC from the HY-1C image was carried out with the simple model and the new model; the results are shown in Figures 4 and 5. To qualitatively analyze the influence of suspended sediment on the new model, three regions were selected for comparative analysis based on the SSC from remote-sensing retrieval: (a) coast, (b) off the coast and (c) far away from the coast. The three water bodies had different SSCs. The SSC in the region (a) was higher than in the other two regions.

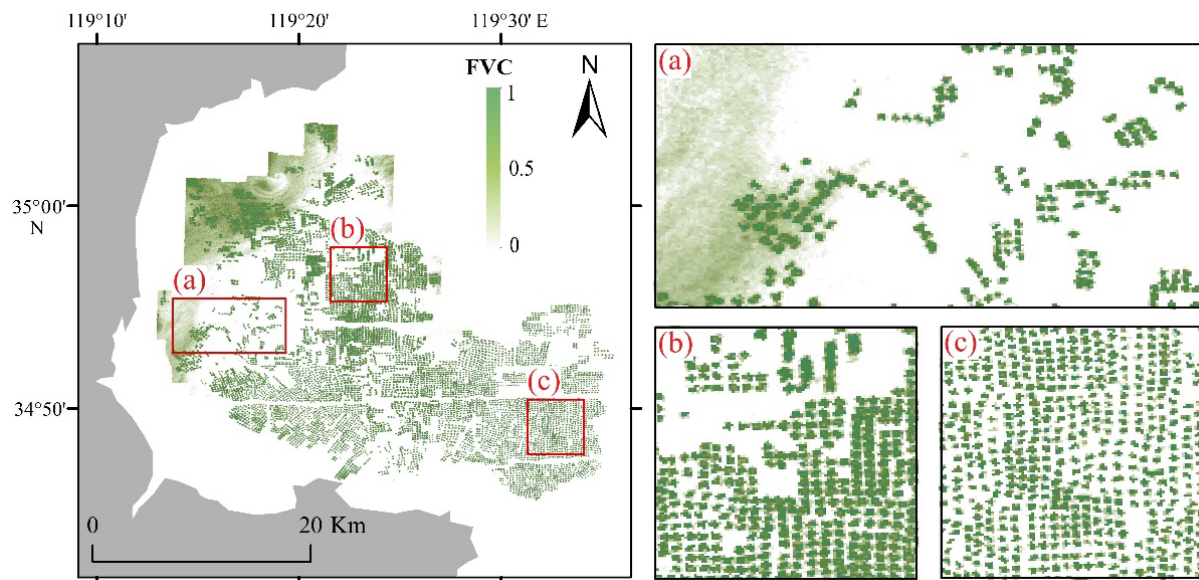


Figure 4. FVC retrieved by simple model on 31 January 2020 in different sea region, (a) coast, (b) off the coast and (c) far away from the coast. FVC is short for fractional vegetation cover and shows that part of one pixel of HY-1C image is covered by *Porphyra*.

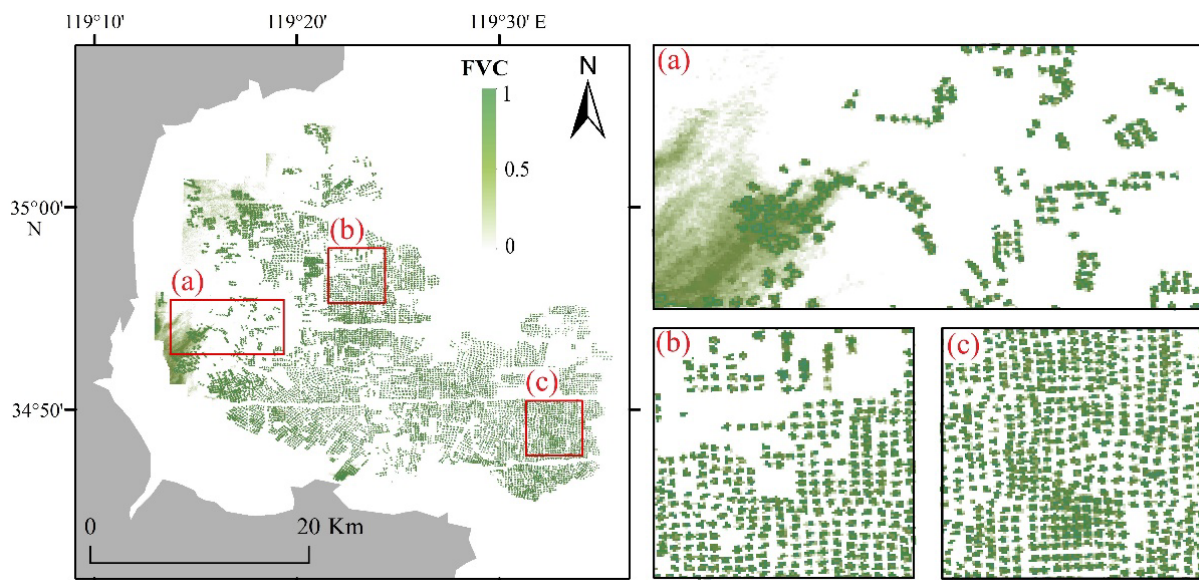


Figure 5. FVC retrieved by the new model on 31 January 2020 in different sea region, (a) coast, (b) off the coast and (c) far away from the coast.

As shown in Figures 5 and 6, the retrieved FVC distribution of the false *Porphyra* cultivation area from HY-1C becomes significantly less, especially in the northern and western parts, such as region (a) of Haizhou Bay where the SSC is higher, with values more than 400 mg/L (see Figure 3). When the SSC is introduced into the new model, the corner of the northwest region with relative low SSC is removed in (a) compared with the result of the simple model in Figure 4a. However, in the corner of the southwest region, some regions with relative high SSC are identified as *Porphyra* cultivation areas and the magnitudes of the FVC differ between in Figure 4b,c and Figure 5b,c. Visual inspection indicated that the SSC was at work in the retrieval of *Porphyra* cultivation area.

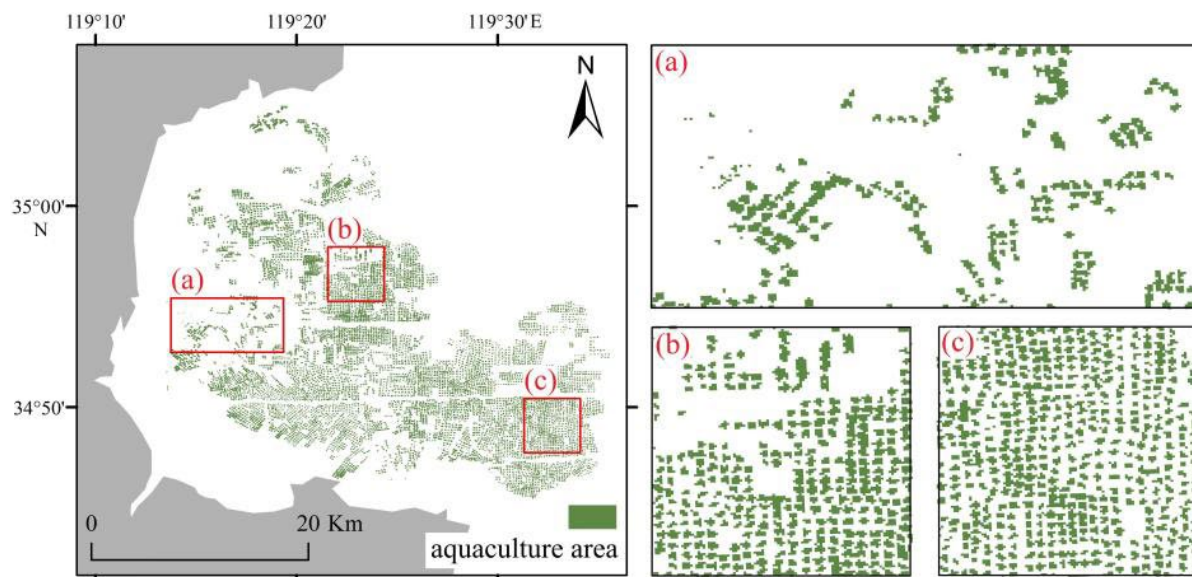


Figure 6. *Porphyra* cultivation area retrieved with random forest model on 31 January 2020 in different sea region, (a) coast, (b) off the coast and (c) far away from the coast. The result was recorded with true or false for each pixel of HY-1C CZI.

Additionally, the new model was qualitatively compared with the random forest model (Figure 6) and pixel-based dichotomy model (Figure 7).

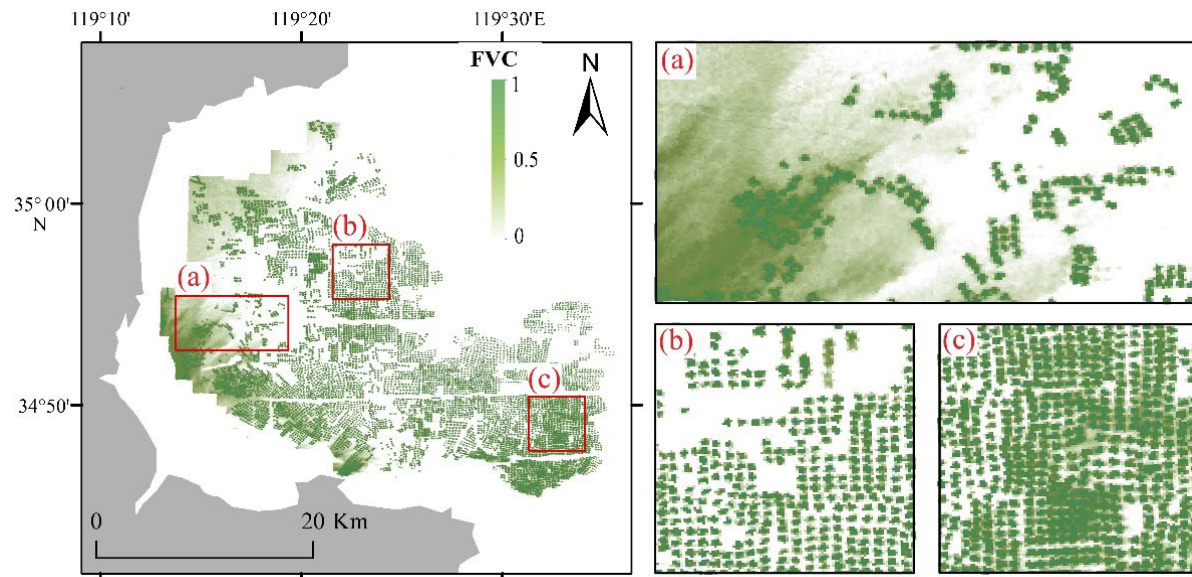


Figure 7. FVC retrieved by the pixel-based dichotomy model on 31 January 2020 in different sea region, (a) coast, (b) off the coast and (c) far away from the coast.

From Figures 5–7, the area of *Porphyra* farming with the new model is mostly between the results of the random forest model and the pixel-based dichotomy model, using the same HY-1C image. In terms of the qualitative distribution, the result with the new model is greater than that with the random forest model and less than that with the pixel-based dichotomy model.

In the higher SSC region, the pixel-based dichotomy model easily misidentifies the seawater with more sediment as *Porphyra* cultivation area (Figure 7a). In contrast, the random forest model has a higher rate of identification in the clear water (Figure 6b,c) and

removed most of the higher SSC region in Figure 6a. The summed area of the *Porphyra* cultivation area appeared to be smaller than in other models.

The result of the new model lies between the two: less than that of the pixel-based dichotomy model and greater than that of the random forest model. The biggest difference of the results with the models was in the higher SSC sea regions. Therefore, the SSC plays an important role of the retrieval of the *Porphyra* cultivation area from the HY-1C image. Furthermore, this effect on the new model still needs quantitative analysis, presented in the next section of the paper.

3.3. Accuracy Analysis of New Model

To quantitatively analyze the accuracy and precision of the new model, the remaining 40% of sample points were employed to validate and compare the results. It is worth noting that although there was a huge number of image pixels for the two kinds of remote-sensing images, each pixel of the HY-1C image has a discrete value between 1/25 and 1, and the value is an integral multiple of 1/25. Thus, based on the 25 values from the HY-1C image, we calculated the average FVC from all the corresponding Sentinel-2 pixels for each value. Finally, 25 average values were acquired from the Sentinel-2 as observed values to assess the models. The results of the three models, excepting the random forest model, are plotted in Figure 8.

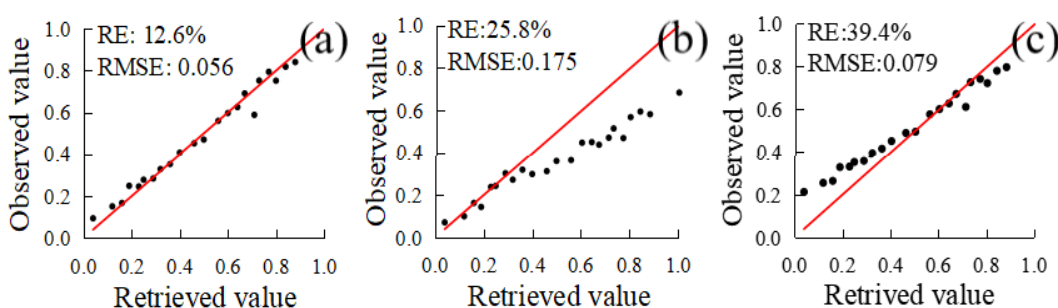


Figure 8. Comparison of FVC retrieved from (a) the new model, (b) the pixel-based dichotomy model, and (c) the simple model. The red solid lines denote the function $y = x$.

From Figure 8, the RE and RMSE of the FVC obtained from the new and simple models are smaller than those from the pixel-based dichotomy model, especially the new model considering the SSC, where the RE and RMSE of the new model are the smallest and their values are 12.6% and 0.056, respectively, followed by the pixel-based dichotomy model. The RE and RMSE of the simple model are the largest of the three and their values are 39.4% and 0.079, respectively. What is more, the FVC data points derived from the new model are uniformly distributed around the function $y = x$, while the others are more biased and only differ in coordinate position. It is worth noting that the results of the random forest classification model are two-value and give only 0 or 1 for the *Porphyra* cultivation area pixels of the HY-1C image; the summed area was taken as the comparative parameter in Haizhou Bay.

Based on Formula (9), the total areas of *Porphyra* cultivation were extracted from the Sentinel-2 image on 31 January 2020 by visual interpretation and from HY-1C satellite images on 31 January 2020 with different models, as shown in Table 4.

Table 4. *Porphyra* cultivation area retrieved with different models.

Methods	Area/km ²	RE/%
Observed value	116.9	
New model	134.3	15
Simple model	144.7	24
Pixel-based dichotomy model	151.2	29
Random forest classification	72.9	37

As shown in Table 4, the new model has the smallest RE of 15% in the total area of *Porphyra* cultivation, followed by the simple model, the pixel dichotomy model, and the random forest model. The three REs are 24%, 29%, and 37%, respectively. This is consistent with the previous qualitative analysis in Figure 8. Meanwhile, the REs of the new model considering the SSC are reduced by 9%, 14%, and 22% compared with those using the simple model, the pixel dichotomy model, and the random forest classification model. Additionally, only the total area extracted by the random forest classification model decreased from that observed from the Sentinel-2 image, while the results of the other three models increased in magnitude.

Generally, the new model was the best for *Porphyra* cultivation area monitoring, and effectively improved the retrieved accuracy with suspended sediment considered.

3.4. Effect of Suspended Sediment on New Model

In order to analyze the influence of SSC on the new model, this paper selects two sea regions for comparative analysis in Figure: (I) the region with SSC more than 500 mg/L and (II) the region with SSC less than 400 mg/L. Then, FVCs were retrieved from the HY-1C satellite image on 9 February 2020, and compared with the observed values by artificial translation from the Sentinel-2 image on 16 February 2020. Based on the different SSCs, sensitivity experiments were carried out.

Similarly, RE and RMSE were used to quantify the retrieved results of *Porphyra* cultivation areas in two different sea regions. Thus, 10,000 sample points from the HY-1C image in each sea region and the total area were applied to evaluate the models, as shown in Table 5.

Table 5. Errors of the retrieved *Porphyra* cultivation areas in different SSC regions.

Sea Region	Method	Total Area (km^2)	RE in Area (%)	RE in Validation Points (%)	RMSE in Validation Points
I	Observed value	3.26	—	—	—
	New model	3.36	3	6	0.102
	Simple model	4.78	47	16	0.173
	Pixel-based dichotomy model	7.18	120	35	0.405
	Random forest classification model	2.67	18	—	—
II	Observed value	3.41	—	—	—
	New model	3.30	3	8	0.089
	Simple model	3.25	5	14	0.152
	Pixel-based dichotomy model	3.59	5	17	0.149
	Random forest classification model	2.94	14	—	—

From Table 5, the RE and RMSE from the sample points or the overall areas with the new model are the smallest among the four models in the two regions, and the accuracy of the random forest classification algorithm is the worst among the models in *Porphyra* cultivation area from the HY-1C image.

In the turbid water with SSC more than 500 mg/L (sea region I), the new model has only 3% RE in the total *Porphyra* cultivation area. The pixel-based dichotomy model has the largest RE and RMSE; its values are 120% in area, 35% in sample points, and 0.405 in sample points, respectively. The accuracy of the simple model is between the new model and the pixel-based dichotomy. However, in clear water (sea region II) with SSC less than 400 mg/L, the advantage of the new model over the simple model and pixel-based dichotomy model is not obvious, although the new model is a bit better in *Porphyra* cultivation area than others. The simple model and pixel-based dichotomy model have similar RE of about 5% and REMS of about 0.15 in validation points.

Obviously, the SSC had an important effect on the retrieval from the HY-1C image, and when considering suspended sediment, the new model had a significant advantage on turbid seawater. However, in clear water, the simple model and pixel-based dichotomy model were exact enough to be employed for monitoring *Porphyra* cultivation area from HY-

1C CZI, although the new model had a small improvement in accuracy. We paid attention to the fact that the random forest model maintained almost constant accuracy wherever *Porphyra* cultivation areas were located and removed almost all the pixels contaminated by high suspended sediment. Therefore, the result of *Porphyra* cultivation area retrieved by the random forest model is always a bit low for HY-1C CZI.

In order to better understand the results retrieved from HY-1C by the models, their distributions in sea region I and II (Figure 3) were plotted in Figures 9 and 10, respectively.

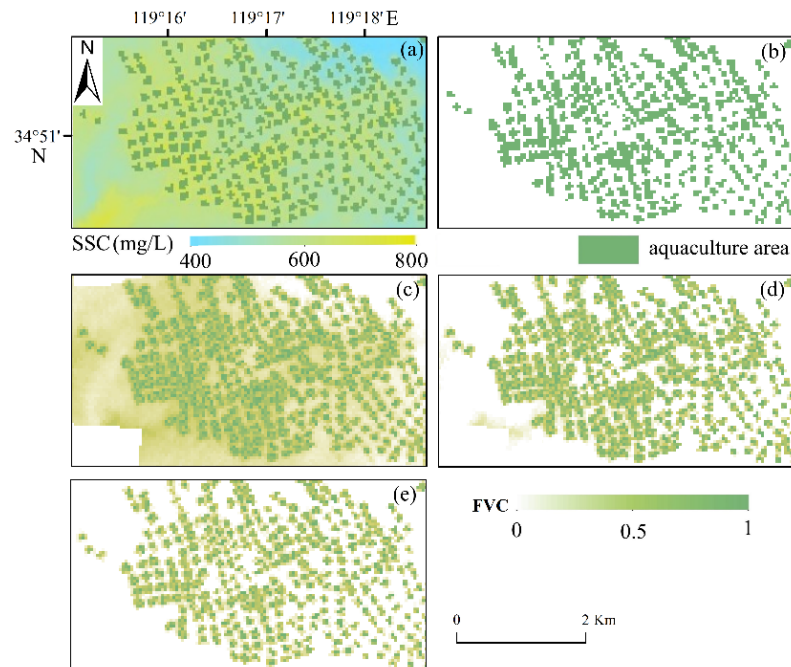


Figure 9. Sea region I distribution of (a) the SSC and observed FVCs, and the results retrieved by the (b) random forest model, (c) pixel-based dichotomy model, (d) simple model, and (e) new model.

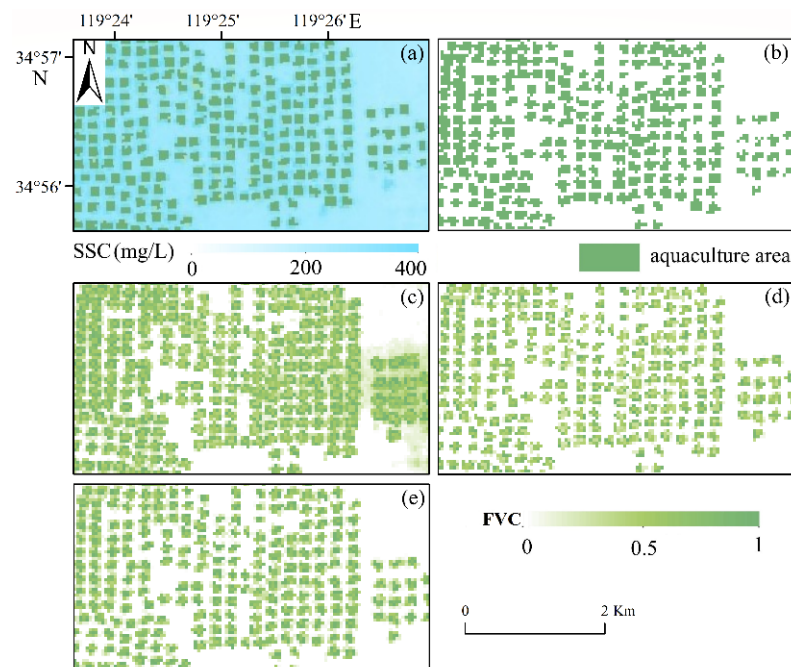


Figure 10. Sea region II distribution of (a) the SSC and observed FVCs, and the results retrieved by the (b) random forest model, (c) pixel-based dichotomy model, (d) simple model, and (e) new model.

In sea region I, Figure 9a shows the distribution of the SSC obtained from the HY-1C image and *Porphyra* cultivation area derived from the Sentinel-2 image, where there are obvious higher SSCs of values between 400 and 800 mg/L. For the pixel-based dichotomy model, fractional high-concentration suspended sediment cover was distinctly misidentified as *Porphyra* cultivation area (Figure 9c), which caused errors in contrast with Figure 9a, and for the simple model, fuzzy object edges led to inaccuracy of identification of *Porphyra* cultivation area causing some parts of the SST area neighboring *Porphyra* cultivation area to be taken as the true value (Figure 9d), which was main cause of the increasing error in total area for HY-1C CZI. The new model expressed excellent ability to find features of *Porphyra* cultivation areas and distinguished almost all pixels of *Porphyra* from turbid seawater in the HY-1C image.

In the clear water of sea region II, which contained little suspended sediment (Figure 10a), there is almost no obvious difference in visual interpretation from the HY-1C image, and the pictures differ in detail, such as in Figure 10c,d. The results retrieved by the pixel-based model contain fuzzy object edges and those from the simple model have the lower FVC for the *Porphyra* culture raft net area, which caused the main remote-sensing retrieval error for HY-1C CZI. From Figures 9b and 10b, results derived by the random forest model always decreased, since this method removes all fuzzy pixels for *Porphyra* cultivation area and includes some suspended sediment.

In a word, the new model considering SSC had excellent ability to detect *Porphyra* cultivation areas from the HY-1C CZI and had the least overall error compared to the other models. The accuracy were improved in monitoring *Porphyra* cultivation area when HY-1C CZI was used.

3.5. Application of New Model in Haizhou Bay

In order to utilize the new model and verify its applicability, four images were used to investigate *Porphyra* cultivation areas in Haizhou Bay. Two kinds of images are listed in Table 2. The comparative results are plotted in Figures 11 and 12.

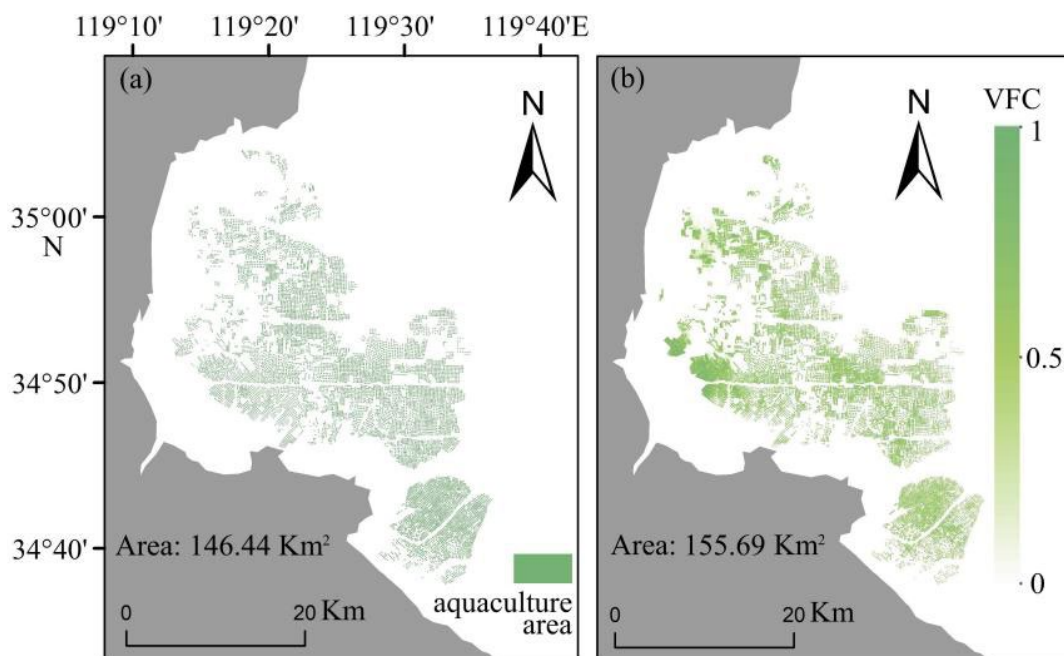


Figure 11. Comparison between (a) observed FVC on 16 February and (b) results retrieved by the new model from the HY-1C image on 9 February 2020.

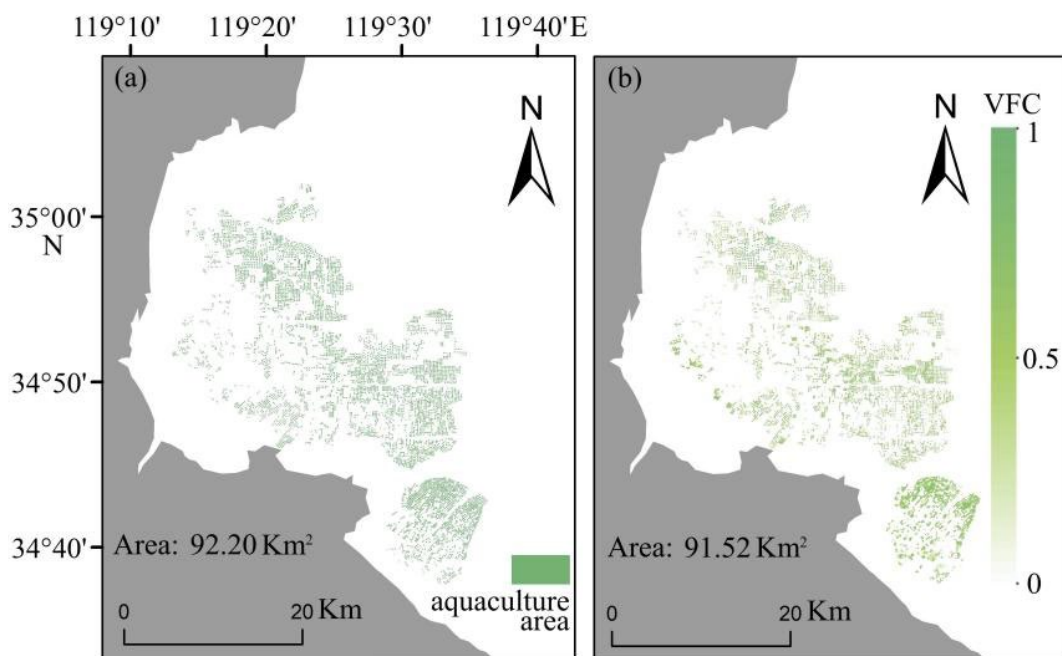


Figure 12. Comparison between (a) observed FVC on 12 March and (b) results retrieved by the new model from the HY-1C image on 19 March 2020.

From Figure 11, *Porphyra* was cultivated in Haizhong Bay and grew well in February 2020, and the *Porphyra* cultivation area is distributed on the coast of Haizhou Bay. Thus, there was relatively higher SSC in the coastal sea, which caused the total difference of 9.25 Km² between the observed and retrieved results from the two different satellite images. In March 2020, some of the *Porphyra*, especially in the coastal region of Hayzhou Bay, had been harvested and the cultivation area decreased from the last month (Figure 12). Thus, the total area difference of *Porphyra* farming between the FVCs retrieved by the new model and the observed values from the Sentinel-2 image decreased by 0.68 Km². The growth stage of *Porphyra* derived by the new model from the HY-1C image was consistent with that found by other methods [42]. The temporal change of total error of the *Porphyra* cultivation area, namely, RE from 6.3% in February to 0.73% in March, indicated that the new model is distinctly sensitive to suspended sediment and that the results are reliable and useful for the coastal sea.

4. Conclusions

For medium-resolution HY-1C images, we employed SSC for model building to retrieve *Porphyra* cultivation area, then constructed a new model in conjunction with high-resolution Sentinel-2 satellite imagery using the linear regression method. Meanwhile, we removed the variable of SSC and established a simple model as contrasting experiment to analyze the effect of SSC. A comparative analysis was performed with the traditional random forest classification algorithm, the pixel-based dichotomy model, and the simple model in different SSC seawater, and some conclusions were drawn.

The SSC has an important influence on retrieval of the coastal *Porphyra* cultivation area. The overall accuracy of the new model was the best of the four models for the HY-1C images, followed by the simple model, the pixel-based dichotomy model, and the random forest classification model. In turbid seawater containing high suspended sediment, the new model eliminated most of the effect of the suspended sediment and obtained the best results for HY-1C CZI. In relatively clear water, the new model was the first choice, but the simple model and the pixel-based dichotomy model were also usable for the HY-1C image. In any seawater, the random forest model was not recommended, and it always gave the smallest area of *Porphyra* cultivation for HY-1C image data.

In conclusion, the new model is preferred for the sea domain comprising regions of *Porphyra* cultivation and suspended sediment for HY-1C satellite imagery. Based on the new model, we can develop quantitative automation technology to process HY-1C images to monitor *Porphyra* spatial distribution in real-time, instead of relying on visual interpretation.

Author Contributions: Conceptualization, Y.C. and Y.H.; methodology, Y.S.; software, Y.S. and M.Z.; validation, Y.C., Y.S. and L.P.; formal analysis, Y.C.; data curation, Y.S.; writing—original draft preparation, Y.C. and Y.S.; writing—review and editing, Y.C. and L.P.; visualization Y.C., M.Z. and Y.S.; supervision, Y.C. and Y.H.; project administration, Y.C.; funding acquisition, Y.C. All authors have read and agreed to the published version of the manuscript.

Funding: The work was supported by the National Natural Science Foundation of China (41776029), National Key Research and Development Program of China (2018YFC1405700), the Six Talent Peaks Project in Jiangsu Province (RJFW-036), the Priority Academic Program Development of the Jiangsu Higher Education Institutions (PAPD) and the Jiangsu Ocean University Initial Scientific Research Fund.

Data Availability Statement: In this study, the HY-1C data were downloaded from National Satellite Ocean Application Center (<https://osdds.nsoas.org.cn> (accessed on 1 May 2020)); Sentinel-2 data were downloaded from the USGS (<https://earthexplorer.usgs.gov> (accessed on 1 May 2020)).

Acknowledgments: The authors would like to thank the creators and archivers of the META dataset used in this study.

Conflicts of Interest: The authors declare no conflict of interest.

References

1. Baweja, P.; Kumar, S.; Sahool, D.; Levine, I. *Seaweed in Health and Disease Prevention*; Academic Press: Amsterdam, The Netherlands, 2016; p. 70.
2. Cheng, T.F.; Zhou, W.F.; Fan, W. Progress in the Methods for extracting aquaculture areas from remote sensing data. *Remote Sens. Land Resour.* **2012**, *3*, 1–5.
3. Fisheries Administration of Ministry of Agriculture and Rural Affairs. *China Fishery Statistical Yearbook 2020*; Agriculture Press: Beijing, China, 2021; p. 72.
4. Lin, H.; Lu, X.; Wang, X.; He, S.; Li, S.; Zheng, W.; Luo, W. Research on spatial expansion mode of laver farming area in Jiangsu province. *Mar. Sci. Bull.* **2021**, *40*, 206–216.
5. Yang, L.; Wang, P.; Cao, L.; Liu, Y.; Chen, L. Studies on charges for sea area utilization management and its effect on the sustainable development of marine economy in Guangdong Province, China. *Sustainability* **2016**, *8*, 116. [[CrossRef](#)]
6. Lu, X.; Zhang, Y.; Zhang, S.; Li, Y. Spatial change analysis of *Porphyra yezoensis* aquaculture in the Lianyungang coastal area by the use of remote sensing and geographic information system technology. *J. Indian Soc. Remote Sens.* **2019**, *47*, 1609–1622. [[CrossRef](#)]
7. Shu, T.; Luo, L.; Wen, Y. Effects of mariculture on coastal ecological environment. *Mar. Environ. Sci.* **2002**, *2*, 74–79.
8. Liu, F.; Feng, S.J. Research advances on green tides in the Yellow Sea. *Adv. Mar. Sci.* **2012**, *30*, 441–449.
9. Yi, J.T.; Huang, J.T.; Song, J.L. Initial understand of enteromorpha prolifera occurred in Yancheng coastal waters in 2008. *Mar. Environ. Sci.* **2009**, *28*, 57–58.
10. Pan, C.; Xia, L.H.; Wu, Z.; Wang, M.; Xie, X.; Wang, F. Remote Sensing Retrieval of Chlorophyll-a Concentration in coastal aquacultivation area of Zhelin Bay. *J. Trop. Oceanogr.* **2021**, *40*, 142–153.
11. Wang, Z.; Xiao, J.; Fan, S.; Li, Y.; Liu, X.; Liu, D. Who made the world's largest green tide in China?—An integrated study on the initiation and early development of the green tide in Yellow Sea. *Limnol. Oceanogr.* **2015**, *60*, 1105–1117. [[CrossRef](#)]
12. Xing, Q.; Wu, L.; Tian, L.; Cui, T.; Li, L.; Kong, F.; Gao, X.; Wu, M. Remote sensing of early-stage green tide in the Yellow Sea for floating-macroalgae collecting campaign. *Mar. Pollut. Bull.* **2018**, *133*, 150–156. [[CrossRef](#)]
13. Xia, Y.; Fan, J.; Li, L.; Li, X. Comparisons on sparse alpine grassland based on vegetation coverage inversion models of remote sensing. *J. Sichuan Agric. Univ.* **2017**, *35*, 37–44+59.
14. Shen, Y.; Liu, J.; Ding, J.; Jiao, J.; Sun, S.; Lu, Y. HY-1C COCTS and CZI observation of marine oil spills in the South China Sea. *Natl. Remote Sens. Bull.* **2020**, *24*, 933–944.
15. Zhang, X.; Wang, H.; Fang, E.J.; Gao, Y.; Guo, B.; Liu, K.; Xu, F.; Chen, W. Preliminary study on the cultivation of *Porphyra* Yezoensis in Bohai Bay. *Mar. Sci. Bull.* **2019**, *2*, 147–152.
16. Zhou, X.; Wang, X.; Xiang, T.; Jiang, H. Method of automatic extracting seaside aquaculture land based on ASTER remote sensing image. *Wetl. Sci.* **2006**, *4*, 64–68.
17. Blaschke, T. Object based image analysis for remote sensing. *ISPRS J. Photogramm. Remote Sens.* **2010**, *65*, 2–16. [[CrossRef](#)]

18. Wu, Y.; Zhang, J.; Tian, G.; Cai, D.; Liu, S. A Survey to aquiculture with remote sensing technology in Hainan province. *Chin. J. Trop. Crops* **2006**, *27*, 108–111.
19. Lin, Q.; Lin, G.; Chen, Z.; Chen, Y. The analysis on spatial-temporal evolution of beach cultivation and its policy driving in Xiamen in recent two decades. *Geo-Inf. Sci.* **2007**, *9*, 9–13.
20. Xu, Y.; Zhang, Z.; Wang, X. Remote sensing monitoring analysis of coastal farming land in Shandong Province in Recent 30 Years. *Earth Inf. Sci.* **2014**, *16*, 482–489.
21. Lu, X.; Gu, Y.; Wang, X.; Lin, Y.; Zhao, Q.; Wang, K.; Fei, X. The identification of *Porphyra* cultivation area by remote sensing and spatial distribution change and driving factors analysis. *Mar. Sci.* **2018**, *42*, 87–96.
22. Wei, Z.; Xing, Q.; Guo, R.; Li, L. Study on the spatial distribution variation of *Porphyra* aquaculture in the southern Yellow Sea during the period 2000–2015 retrieved by satellite remote sensing. *J. Ocean. Technol.* **2018**, *37*, 17–22.
23. He, Q.; Zhou, J.; Yu, S.; Li, C.; Yu, D. Remote Sensing Survey on the Distribution of Cage-Fenced Culture in the Top 10 Reservoirs of Hunan Province based on GF-2 data. *Bull. Surv. Mapp.* **2019**, *10*, 8–11+159.
24. Xu, H.; Zhang, Y.; Zhang, J. Research on the automatic extraction of floating raft aquaculture based on SR-NDVI and median filtering in Lianyungang. *J. Ocean Technol.* **2021**, *40*, 1–8.
25. Wang, X.; Liu, J.; Xing, Q.; Chen, Y. Monitoring of *Porphyra* cultivation dynamics in Lianyungang based on coastal zone image. *Mar. Sci.* **2021**, *45*, 9–17.
26. Chu, J.; Zhao, D.; Zhang, F. Wakame raft interpretation method of remote sensing based on association rules. *Remote Sens. Technol. Appl.* **2012**, *27*, 941–946.
27. Wang, F.; Xia, L.; Chen, Z.; Cui, W. Remote sensing identification of coastal zone mariculture modes based on association-rules object-oriented method. *Trans. Chin. Soc. Agric. Eng.* **2018**, *34*, 210–217.
28. Guo, R. *Evaluation on the Changes in the Seaweed (Porphyra Yezoensis) Aquaculture in Jiangsu Coastal Waters Using Remote Sensing*; University of Chinese Academy of Sciences: Beijing, China, 2017.
29. Xing, Q.; An, D.; Zheng, X.; Wei, Z.; Wang, X.; Li, L.; Tian, L.; Chen, J. Monitoring seaweed aquaculture in the Yellow Sea with multiple sensors for managing the disaster of macroalgal blooms. *Remote Sens. Environ.* **2019**, *231*, 111279. [[CrossRef](#)]
30. Lin, M.; He, X.; Jia, Y. Advances in marine satellite remote sensing technology in China. *Acta Oceanogr. Sin.* **2019**, *41*, 99–112.
31. Kaur, S.; Bansal, R.K.; Mittal, M.; Goyal, L.M.; Kaur, I.; Verma, A.; Son, L.H. Mixed pixel decomposition based on extended fuzzy clustering for single spectral value remote sensing images. *J. Indian Soc. Remote Sens.* **2019**, *47*, 427–437. [[CrossRef](#)]
32. Yang, H.; Deng, F.; Fu, H.; Zhang, J. Estimation of rape-cultivated area based on decision tree and mixed pixel decomposition. *J. Indian Soc. Remote Sens.* **2021**, *49*, 1285–1292. [[CrossRef](#)]
33. Gao, Y.; Pan, Y.; Huang, H.; Mohamed, E.R.; Aly, Z.M. Swarm Intelligence Algorithm for Extracting Spatial Spectrum Features of Hyperspectral Remote Sensing Image and Decomposing Mixed Pixels. *J. Intell. Fuzzy Syst.* **2020**, *39*, 5045–5055. [[CrossRef](#)]
34. Sun, Y.; Gu, Z.; Li, D. Study on remote sensing retrieval of leaf area index based on unmanned aerial vehicle and satellite image. *Sci. Surv. Mapp.* **2021**, *46*, 106–112+145.
35. Pope, R.; Fry, E. Absorption spectrum (380–700 nm) of pure water. II. integrating cavity measurements. *Appl. Opt.* **1997**, *36*, 8710–8723. [[CrossRef](#)] [[PubMed](#)]
36. Hou, P.; Wang, L.; Cao, G.; Yang, F. Analysis and research of remote sensing for suspended sediment in water. *Proc. SPIE Int. Soc. Opt. Eng.* **2004**, *5239*, 89–97.
37. Pereira, R.; Yarish, C. Mass Production of Marine Macroalgae. *Encycl. Ecol.* **2008**, *5*, 2236–2247.
38. Gitelson, A.A.; Kaufman, Y.J.; Stark, R.; Rundquist, D. Novel algorithms for remote estimation of vegetation fraction. *Remote Sens. Environ.* **2002**, *80*, 76–87. [[CrossRef](#)]
39. Markham, B.L.; Barker, J.L. Thematic mapper bandpass solar exoatmospheric irradiances. *Int. J. Remote Sens.* **1987**, *8*, 517–523. [[CrossRef](#)]
40. Paruelo, J.M.; Epstein, H.E.; Lauenroth, W.K. ANPP estimates from NDVI for the central grassland region of the United States. *Ecology* **1997**, *78*, 953–958. [[CrossRef](#)]
41. Xu, H. A Study on information extraction of water body with the modified normalized difference water index. *Natl. Remote Sens. Bull.* **2005**, *5*, 589–595.
42. Cai, L.; Zhou, M.; Liu, J.; Tang, D.; Zuo, J. HY-1C observations of the impacts of islands on suspended sediment distribution in Zhoushan coastal waters, China. *Remote Sens.* **2020**, *12*, 1766. [[CrossRef](#)]
43. Van der Linden, S.; Rabe, A.; Held, M. The EnMAP-box—A toolbox and application programming interface for EnMAP data processing. *Remote Sens.* **2015**, *7*, 11249–11266. [[CrossRef](#)]